Pergamon

Int. J. Solids Structures Vol. 33, No. 11, pp. 1535–1541, 1996

0020-7683/96 $15.00 + .00

0020-7683(95)00112-3

STRESS SINGULARITIES AT TRIPLE JUNCTIONS WITH FREELY SLIDING GRAINS

CATALIN R. PICU and VIJAY GUPTA†
Thayer School of Engineering, Dartmouth College, Hanover, NH 03755, U.S.A.

(*Received* 27 *February* 1995; *in revised form* 21 *April* 1995)

Abstract—Stress singularities at grain triple junctions due to freely sliding grain boundaries in idealized two-dimensional single-phase polycrystals have been analyzed. The shear stress is assumed to be completely relaxed along the grain boundaries while the normal stress is allowed to be fully transmitted. The singularity exponent was found to be independent of the elastic constants of the grains, and for some triple junction configurations, super-singularities (i.e., stronger than the standard -0.5 as found at the tip of a crack in homogeneous material) were obtained. Interestingly, for most geometrical configurations, the solution structure indicates a fixed mode near the triple junction, irrespective of the far-field load combination.

1. INTRODUCTION

Modeling the nucleation of cracks and cavities in engineering polycrystals requires a quantitative description of the stress and strain fields at grain triple junctions or at the apexes of grain boundary particles. In high temperature alloys loaded above $0.4T_m$, the stresses are further concentrated due to freely sliding grain boundaries. By prescribing a linear viscous behavior for the sliding grain boundaries in a power-law creeping alloy, Lau *et al.* (1983, 1984) calculated the stress concentrations at apexes of pinning grain boundary particles and triple junctions of 2D polycrystals with hexagonal grains. The largest singularity value of -0.225 at the apex of a square particle and that of -0.321 at the grain triple junction were obtained for an alloy with an effective creep exponent of 3.

The purpose of this note is to provide stress singularities at *asymmetric* two-dimensional triple grain junctions with random orientations of the grain boundaries, albeit by limiting the deformation in each grain to within their elastic limits. It is further assumed that all grains are isotropic and made out of the same material with elastic modulus E and Poisson's ratio ν. The boundaries are allowed to slide freely with fully relaxed shear stresses, but still allowing the normal traction to be completely transmitted across them. The results provided here can be useful for understanding the deformation of ceramics and other high temperature alloys at relatively high strain rates where the cracks and voids can nucleate under short-range singular stresses before they are relaxed by the creeping grains. In fact, we recently (Picu and Gupta, 1995a) documented such crack nucleation events from triple junctions of columnar freshwater ice due to grain boundary sliding when the samples were loaded under across-column biaxial compression at a strain rate of 10^{-3} s^{-1} at -10°C. Interestingly, even with such local-scale inelastic dissipations, the overall behavior of the polycrystal remained brittle with a sharp termination in its linear compression stress–strain curve. Although a simple model that assumed the sliding grain boundary as an effective mode II crack with a sliding resistance τ_b was formulated to explain the observed cracking events under compression loading (Picu and Gupta, 1995b), the detailed structures of the stress and strain fields at the triple junctions were not analyzed. The same is true for simultaneous sliding of two or more boundaries meeting at a junction. The present paper provides the structure of the stress field at such triple junctions to within a scaling constant k, the generalized stress intensity factor.

† Now at the Mechanical Aerospace and Nuclear Engineering Department, UCLA, Los Angeles, CA 90095-1597, U.S.A.

2. ANALYSIS

Consider the geometry of Fig. 1. The grain boundary positions are defined by the angles α_1 and α_2. The three grains are considered to be made from the same elastic material defined by the Young's modulus E and the Poisson ratio ν. The stress field σ_{ij} very close to the triple junction in each grain is of the separable form, and can be expressed in a polar coordinate system centered at the triple junction as

$$\sigma_{ij}(r, \theta) = kr^{\gamma} f_{ij}(\theta), \tag{1}$$

where γ is the singularity exponent, $f_{ij}(\theta)$ are angular functions and k is a scaling constant. The boundary conditions are defined by the continuity of the normal displacement u_θ and stress $\sigma_{\theta\theta}$ across each boundary in Fig. 1, whereas, consistent with the assumption of freely sliding grain boundaries, the shear stress along each interface is zero.

The problem posed above is directly amenable to the standard Williams-type singularity analysis (Williams, 1952) which provides γ and $f_{ij}(\theta)$ but not the amplitude factor k, for which the full problem including the external loading must be considered. In the local field analysis, γ is obtained as the eigenvalue of a 12×12 system of equations that result upon the use of the above boundary conditions. The exponent γ was searched numerically in the domain $-1 < \gamma < 0$, since $\gamma > 0$ leads to non-singular fields, whereas $\gamma < -1$ leads to physically impossible strain energy densities in the continuum. Interestingly, the elastic constants E and ν do not enter the eigenvalue problem. Thus, the eigenvalues and the associated eigenvectors depend only on the two parameters α_1 and α_2 defining the geometry of the triple junction. The solution structure allows for two negative eigenvalues γ_1 and γ_2, *each* corresponding to *only one* eigenvector instead of two, as observed for the standard crack tip fields. The singular part of the local stress field can be written as

$$\sigma_{ij}(r, \theta) = k_1 r^{\gamma_1} f_{ij}^1(\theta) + k_2 r^{\gamma_2} f_{ij}^2(\theta). \tag{2}$$

Near the triple junction, however, only the most singular term dominates. Unlike most standard fracture problems, $f_{ij}^1(\theta)$ and $f_{ij}^2(\theta)$ here represent a *fixed* mode θ-variation which depends upon the geometrical parameters α_1 and α_2, and are independent of the far-field loading combination. This behavior was also observed by He and Hutchinson (1989) for cracks impinging at an oblique angle to an interface between two dissimilar isotropic elastic solids. As suggested by these authors, the dominance zone for such a field is rather limited.

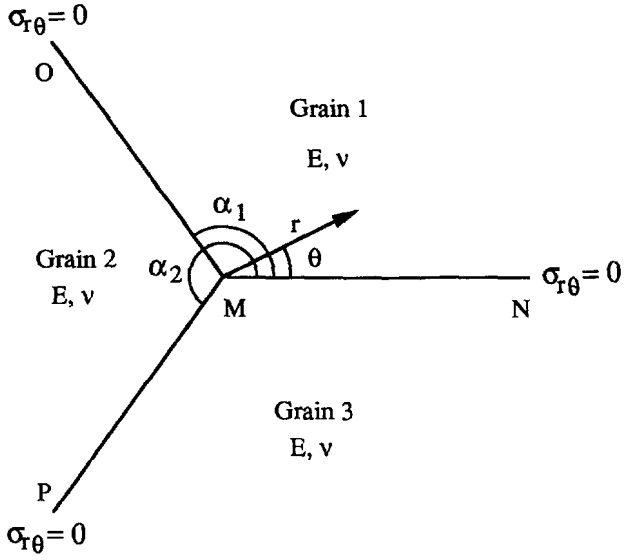

Fig. 1. Details of the geometry at a grain triple junction.

3. RESULTS

Figure 2a shows the contours of the singularity exponent γ in the α_1–α_2 plane for the case where all grain boundaries are allowed to slide. When drawing the singularity map, several symmetries of the geometry in Fig. 1 have been considered. As discussed below it is only necessary to consider the geometrical configurations represented within the triangular region BCD, since there exists a *regular* mirror symmetry about the line BD, and a *specific* mirror symmetry about the line EB where only the lines parallel to the α_2 axis are reflected by the mirror EB. The reasons for these symmetries are discussed below.

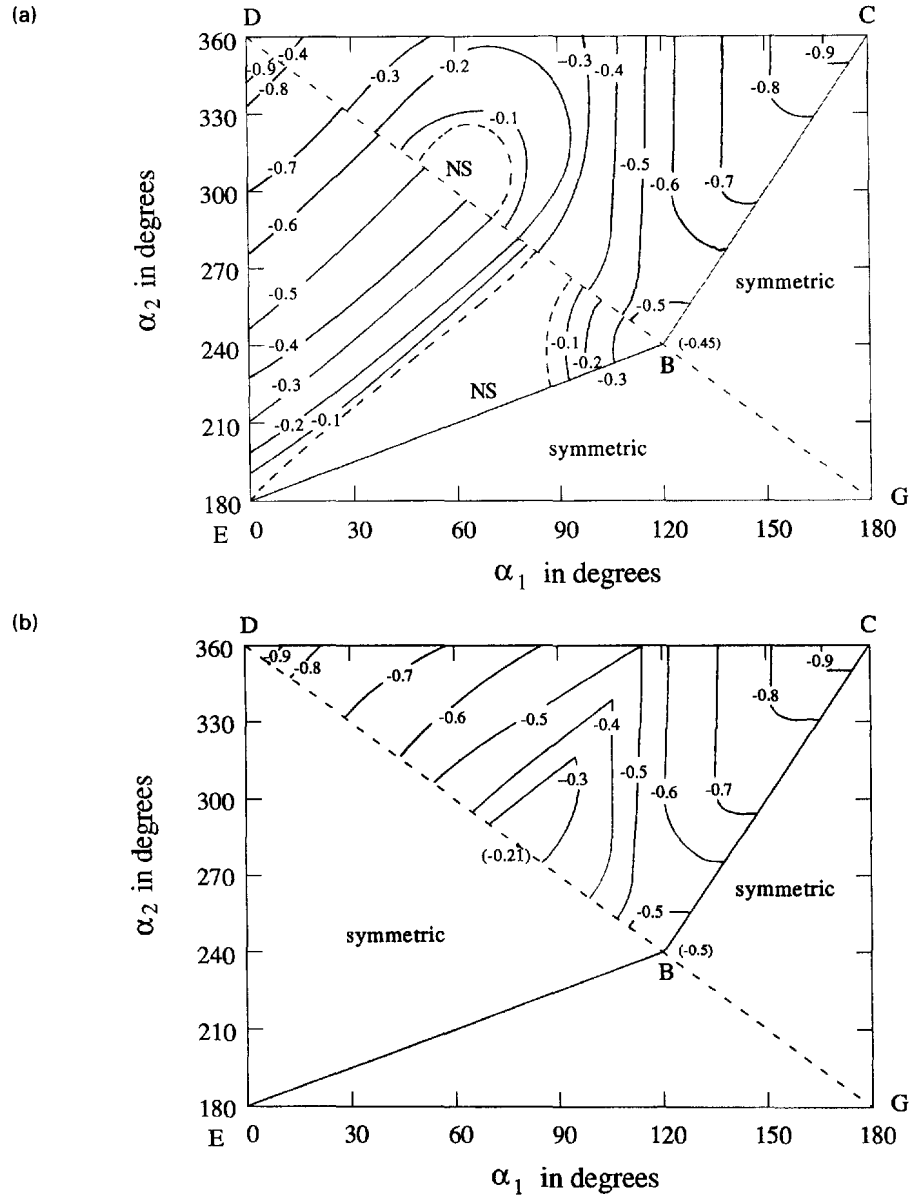

Fig. 2. (a) Contours of the singularity exponent γ in the α_1 and α_2 plane. The upper region of the map BCD shows the singularities corresponding to the first eigenvalue (γ_1), while the lower region BDE corresponds to the second eigenvalue (γ_2). The values of γ_1 and γ_2 in other configurations can be simply obtained by using the regular mirror symmetry along the line BD, and special symmetries along the lines BC and BE where only the lines parallel to the α_1 and α_2 axes are reflected in a mirror-like fashion, respectively. NS marks a region corresponding to nonsingular configurations. At point B, the value in parentheses represents the singularity corresponding to a double eigenvalue. All singularity exponents are independent of the elastic constants. (b) Contours of the leading singularity exponent $\gamma = \max(\gamma_1, \gamma_2)$ in the α_1–α_2 plane. γ assumes its smallest value for the symmetric configuration defined by $\alpha_1 = 79°$.

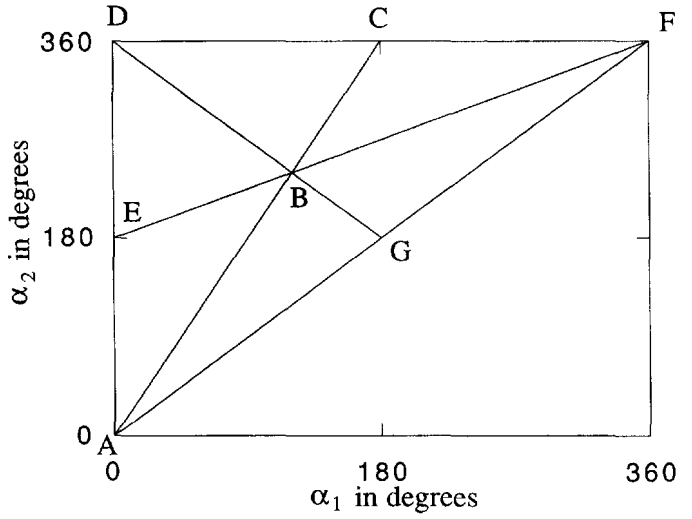

Fig. 3. A schematic representation of the various symmetries expected for the singularity exponent in the α_1–α_2 plane. These essentially result from the invariance of the grain configuration upon a 180° rotation of the geometry about the grain boundaries MN, MO and MP in Fig. 1.

To cover all possible geometrical configurations in Fig. 1, α_1 should take values in the range $0° < \alpha_1 < 360°$, whereas α_2 varies in the interval $\alpha_1 < \alpha_2 < 360°$. This represents the region AFD above the line AF defined by $\alpha_1 = \alpha_2$ in Fig. 3. It can be seen from Fig. 1 that a 180° rotation of the assembly about the grain boundary MN would preserve the magnitude of the angles between the boundaries, and should yield an identical geometrical configuration. If α_1', α_2' are the corresponding angles for the boundaries MO and MP in the rotated configuration, they will be related to their unrotated counterparts through: $\alpha_1' = (2\pi - \alpha_2)$ and $\alpha_2' = (2\pi - \alpha_1)$. This represents a mirror symmetry about the line DG in Fig. 3. The above argument also holds for a 180° rotation about the grain boundary MO, and for this case, with respect to the coordinate frame in Fig. 1, the new angles α_1', α_2' are related to α_1 and α_2 via: $\alpha_1' = \alpha_1$ and $\alpha_2' = (2\pi - \alpha_2 + \alpha_1)$. This represents a special mirror symmetry along the line $\alpha_2 = \pi + \alpha_1/2$, which is plotted as line EF in Fig. 3. The word "special" is used to indicate that only those lines that are parallel to the α_2 axis would reflect in a mirror-like fashion with respect to the line EF. A similar special mirror symmetry exists along the line AC in Fig. 3, which results through a 180° rotation of the geometry in Fig. 1 around the grain boundary MP. Here, only the lines parallel to the α_1 axis reflect in a mirror-like fashion with respect to the line AC.

Based on the above, it appears that one needs to consider only the region BCD to generate results for all geometrical possibilities. As discussed earlier, two eigenvalues were obtained for each geometrical configuration (α_1, α_2). To represent the solutions in a compact form, we show the first set of eigenvalues in the triangular region BCD, whereas the second one in the pair is shown in the region BDE. The data at points E, D, and C have no physical meaning since the corresponding geometries cannot be in equilibrium under an applied load. Upon a quick glance at the singularity map, it is evident that there are many configurations that yield super-singularities, i.e. those greater than the standard -0.5 as obtained at the tip of a crack in homogeneous media.

As discussed earlier, only the strongest singularity characterizes the stress field close to the triple junction. Figure 2b shows the leading eigenvalue γ ($= \max(\gamma_1, \gamma_2)$) for all configurations explored in Fig. 2a. While in most cases γ is a super-singularity, for geometries defined by $60° < \alpha_1 < 100°$ and $240° < \alpha_2 < 330°$, singularities weaker than -0.5 are obtained, with a minimum value of -0.21 corresponding to the symmetric case with $\alpha_1 = 79°$.

Figures 4(a) and (b) show the eigenvectors associated with the eigenvalues γ_1 and γ_2, respectively, corresponding to the geometrical configuration defined by $\alpha_1 = 80°$ and

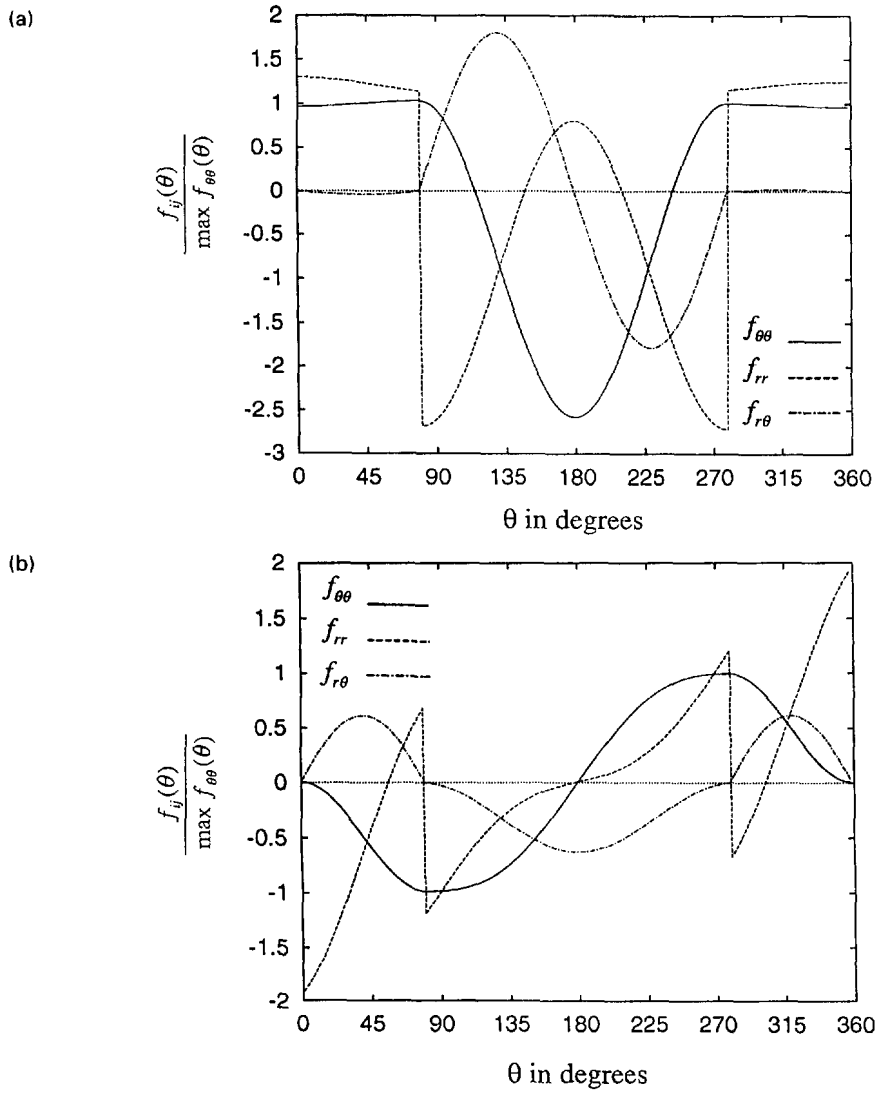

Fig. 4. Eigenvectors associated with the eigenvalues γ_1 (a) and γ_2 (b) for the geometrical configuration defined by $\alpha_1 = 80°$ and $\alpha_2 = 280°$. Since only one field is obtained for each eigenvalue, a fixed mode near the triple junction, irrespective of the applied far field load, is implied.

$\alpha_2 = 280°$. The ordinate in Fig. 4 is normalized with respect to the absolute maximum of $f_{\theta\theta}(\theta)$. Interestingly, for symmetric grain configurations (as considered in Fig. 4), it was found that each of the two eigenvectors are symmetric and antisymmetric with respect to a mirror-line of the configuration. For the geometry shown in Fig. 4, this line is located at $\theta = 180°$ with Fig. 4(a) containing the symmetric and Fig. 4(b) depicting the antisymmetric field. This relationship between the two is surprising, and of course is of a very different nature than the double eigenfields (bearing the same relationship) obtained for the homogeneous crack problem, where a linear combination of the two satisfies the equilibrium with the applied far-field loads.

The normal stress across the grain boundaries is of interest for addressing the issue of crack nucleation, and as shown in Fig. 4, the stress can become tensile to support the nucleation of cracks. For almost all configurations, the maximum tensile $\sigma_{\theta\theta}$ stress of the symmetric field is obtained along one of the bisectors of the three angles spanned by the grain boundaries, whereas for the antisymmetric field $\sigma_{\theta\theta}$ is maximum along the grain boundaries. A quantitative evaluation of the nucleation process, however, requires the calculation of the amplitude factors k_1 and k_2 in eqn (2) (Picu *et al.*, 1994).

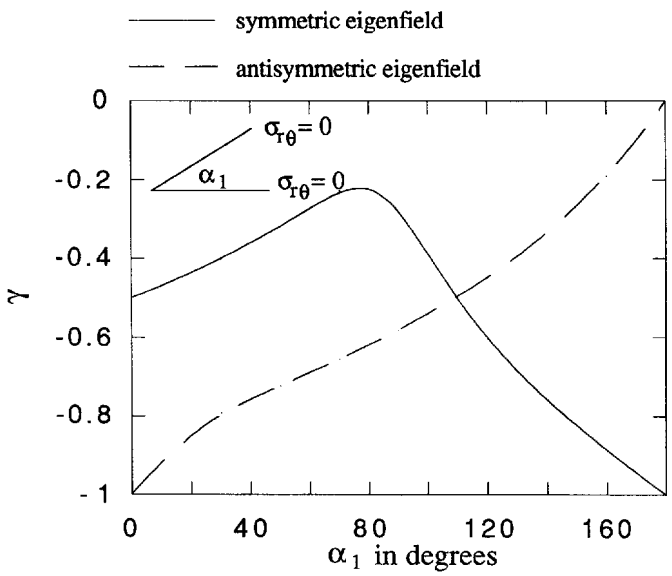

Fig. 5. The singularity exponents γ_1 and γ_2 as a function of α_1 when only two boundaries are allowed to slide. The case of $\alpha_1 = 0$, corresponds to a single sliding grain boundary, for which $\gamma_1 = -0.5$.

An exception to the above fixed mode eigenfields was the case represented by the fully-symmetric grain configuration with $\alpha_1 = 120°$ and $\alpha_2 = 240°$. For this case, a double eigenvalue of -0.45 was obtained which yielded two linearly independent eigenvectors, each of which can be taken as symmetric and antisymmetric with respect to the mirror line for the grain configuration. Here, the relationship between the two fields is akin to that for the standard crack problem.

When only two favorably oriented grain boundaries are activated by the applied shear stress and are free to slide, all possible geometries can be obtained in terms of only one geometrical parameter α_1 measured with respect to a coordinate frame whose x_1-axis is aligned with one of the sliding grain boundaries. This is depicted in the inset of Fig. 5. As before, two eigenvalues with each corresponding to only one eigenvector were obtained. Figure 5 shows the variation of the singularity exponents γ_1 and γ_2 as a function of α_1, whereas Figs 6(a) and (b), respectively, show the associated eigenfields for γ_1 and γ_2 for a specific grain configuration defined by $\alpha_1 = 140°$. For these geometries, the two eigenfields are antisymmetric and symmetric with respect to the line that bisects the two sliding boundaries. As for the case with three sliding boundaries, this relationship between the two fields is different from that obtained in the standard fracture problems. For the case of $\alpha_1 = 0$, corresponding to only one sliding grain boundary, an eigenvalue of -0.5 was obtained, since the sliding boundary behaves essentially as a mode II crack.

4. CONCLUSIONS

Stress singularities at two-dimensional grain triple junctions for the case where one, two and all three grain boundaries were allowed to slide freely, were obtained. The deformation within each grain was limited to isotropic elastic behavior. The key features of the stress field involve not only the super-singularities for certain grain configurations, but also the associated eigenfields indicate a fixed mode near the triple junction.

The utility of the current results lies in addressing the problem of crack nucleation in polycrystals deformed at high homologous temperature, but loaded at relatively high strain rates. Under such conditions, it is possible to nucleate cracks under the short-range stresses before they are relaxed due to creep. Such events were documented by us in ice polycrystals (Picu and Gupta, 1995a). The reader is referred to Picu *et al.* (1994) to see how the information given here can be synthesized to study quantitatively the problem of crack nucleation.

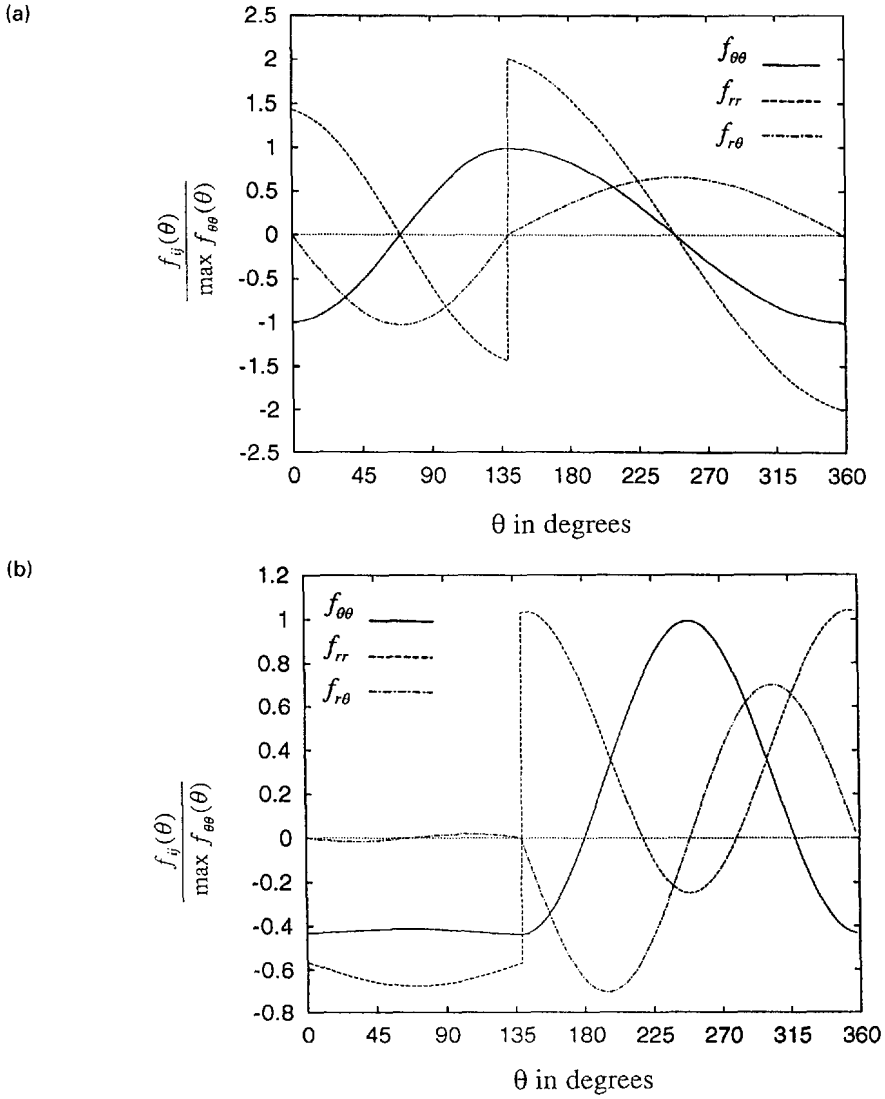

Fig. 6. Eigenvectors of the antisymmetric and symmetric fields associated with the eigenvalues $\gamma_1 = -0.33$ (a) and $\gamma_2 = -0.76$ (b) for the geometrical configuration defined by $\alpha_1 = 140°$. The eigenfields are normalized with respect to the absolute maxima of the $f_{\theta\theta}$ field.

Acknowledgments—This work is being supported by the ONR grant no. N00014-92-J-1247 for which we are grateful to Drs Y. D. S. Rajapakse, Steve Ramberg and Tom Curtin of that agency.

REFERENCES

He, M. Y. and Hutchinson, J. W. (1989). Crack deflection at an interface between dissimilar elastic materials. *Int. J. Solid Struct.* **25,** 1053–1067.

Lau, C. W., Argon, A. S. and McClintock, F. A. (1983). Application of the finite element method in micro-mechanical analyses of creep fracture problems. *Comput. Struct.* **17,** 923–931.

Lau, C. W., Argon, A. S. and McClintock, F. A. (1984). Stress concentrations due to sliding grain boundaries in creeping alloys. *Special Technical Publication* 803, Vol. 1, pp. 551–572. American Society For Testing and Materials (ASTM), Philadelphia.

Picu, C. R. and Gupta, V. (1995a). Observations of crack nucleation in columnar ice due to grain boundary sliding. *Acta Metall. Mater.* (in press).

Picu, C. R. and Gupta, V. (1995b). Crack nucleation in columnar ice due to elastic anisotropy and grain boundary sliding. *Acta Metall. Mater.* (in press).

Picu, C. R., Gupta, V. and Frost, H. J. (1994). Crack nucleation mechanism in saline ice. *J. Geophys. Res.* **99B,** 11775–11785.

Williams, M. L. (1952). Stress singularities resulting from various boundary conditions in angular corners of plates in extension. *J. Appl. Mech.* **19,** 526–528.